



Synthesis and Characterization of Color Tunable Europium(III) and Terbium(III) Co-Doped LaSrAl₃O₇ Nanocrystalline Phosphors: A Photoluminescent Synergy

DEEPIKA DHATERWAL¹, MAHESH MATORIA¹, ANNU DALAL¹, SURENDER KUMAR¹ and SONIKA SINGH^{1*}

Department of Chemistry, Chaudhary Bansi Lal University, Bhiwani-127031, India

*Corresponding author: E-mail: sonikasinghdhanger@cblu.ac.in

Received: 10 June 2024;

Accepted: 12 July 2024;

Published online: 25 July 2024;

AJC-21716

Color tunable La_{0.99-x}Eu_xTb_{0.01}SrAl₃O₇ ($x = 0.01-0.07$ mol) luminous nanocrystalline materials were synthesized using an affordable, simple, streamlined and self-propagating, urea-assisted solution combustion synthesis route. The X-ray powder diffraction pattern of optimized La_{0.95}Eu_{0.04}Tb_{0.01}SrAl₃O₇ co-doped phosphor sintered at 900 °C revealed the formation of single phased phosphor having tetragonal crystalline structure with $P42_1m$ (113) space group. The field emission scanning electron microscopy (FESEM) and transmission electron microscopy (TEM) micrographs revealed agglomerates featuring spherical-shaped porous nanoparticles with interconnect boundaries and smooth surface. The basic composition was determined *via* scrutiny of energy dispersive X-ray (EDAX) spectrum. Observations of diffuse reflectance spectroscopy were analyzed to determine the optical band gap values of synthesized Eu³⁺/Tb³⁺ co-doped LaSrAl₃O₇ nanocrystalline luminescent materials. To explore how dopant concentration affected the luminous intensity of phosphors, a thorough examination of the photoluminescence excitation and emission spectra of La_{0.99-x}Eu_xTb_{0.01}SrAl₃O₇ ($x = 0.01-0.07$ mol) was executed. The analysis of luminescence spectra demonstrated that Tb³⁺ efficiently sensitized the Eu³⁺ ion. The critical distance (R_c) was calculated to be 5.576 Å and it emerged that non-radiant energy loss occurrence *i.e.* concentration quenching observed after $x = 0.04$ mol (Eu³⁺) doping in La_{0.99-x}Eu_xTb_{0.01}SrAl₃O₇ ($x = 0.01-0.07$ mol) co-doped phosphors was induced by the dipole-quadrupole (d-q) interactions. Moreover, colorimetric attributes including Commission International de l'Eclairage 1931 color coordinates (x, y), color purity and correlated color temperature were obtained by utilization their emission data. The derived nanophosphor materials photometric traits enable new design opportunities for upgraded luminous materials that can be utilized in field emission displays, diverse luminous sources, photonic appliances, phosphor converted light emitting diodes, full-color displays and numerous lighting devices.

Keywords: Solution combustion, Nanophosphors, Photoluminescence, Color coordinates, Tunable.

INTRODUCTION

In recent era, phosphor converted light emitting diodes (pc-LEDs), which have remarkable luminance efficiency and an assortment of emission shades, have garnered significant attention as an accessible and environmentally sustainable source of illumination [1,2]. Multicolor emissions through a single host matrix phosphor and chip combo seem more feasible and can address the reabsorption issue as compared to ultraviolet light emitting diodes (UV-LED's) that use diverse essential phosphor mixes [3-5]. Consequently, the need is imperative to produce the color-tunable luminescent material with single host lattice. The key benefit of single-phase color tunable emitting phosphors over multicomponent emitting devices is their ability to simultaneously improve the rendering index of illumination and

produce multicolor emission at low color temperatures [6]. Owing to their superior chemical stability, prolonged emission life span, acute bandwidth, tunable illumination hue and significant luminescence efficacy, rare-earth ions doped nanophosphor materials have achieved extensive use in various areas in the recent few years, including illumination, displays, luminescence materials for biological applications, white light emitting diodes (WLEDs) as well as various kinds of sensors for analysis [7-10]. The photoluminescent materials exhibiting the required vibrant color impact could potentially be produced by changing the dopant, content of dopant and utilising rare-earth ions combos in tandem with an appropriate host [11,12]. It has been suggested that unique luminous patterns could potentially be achieved by incorporating co-dopants in single hosts as multiple energy transfer (ET) exhibits fascinating multicolor emission.

As luminosity could potentially be regulated through the energy conveyed by doped/co-doped lanthanides *e.g.* terbium (III) and europium(III) ions draw significant emphasis because of their extended luminescence endurance and confined emission lines inside the visible realm. The activator, Eu^{3+} is known for its red color emission correspond to the transitions ${}^5\text{D}_0 \rightarrow {}^7\text{F}_j$ whereas the ions Tb^{3+} exhibit green emission lines that correspond to the transitions ${}^5\text{D}_4 \rightarrow {}^7\text{F}_j$ [13]. The practical application of luminescent materials that contain Eu^{3+} is, however, limited by the fact that their absorption peak percentage relatively modest and slightly limited in the ultraviolet (UV) range. In phosphors, the transfer of energy is a fundamental phenomenon that could take place among doped ion pairs (sensitizer/activator) as well as from the host system to the doped ions [14]. The co-doping approach, which involves the simultaneous incorporation of various luminescent ions into the host lattice, has garnered significant attention in recent years. This strategy has the potential to improve the material's luminescence properties in a synergistic manner, leading to increased color purity, increased emission intensity, and an extended wavelength range. Exploring the consequences of sensitization and the co-doping energy transfer mechanism may assist to address this issue in the future. The energy transferred from $\text{Tb}^{3+} \rightarrow \text{Eu}^{3+}$ is beneficial since Eu^{3+} absorption wavelength and Tb^{3+} emission wavelength are quite in proximity to one another.

Substantial study has been put towards investigating the energy transfer process, luminescent properties and tailored full-color illuminating luminous materials co-doped with Tb^{3+} and Eu^{3+} , *i.e.* $\text{SrLaGa}_5\text{O}_7$ [14], $\text{ZnLaB}_5\text{O}_{10}$ [15], $\text{Li}_3\text{Lu}_3\text{Te}_2\text{O}_{12}$ [16], $\text{Ca}_4\text{La}_6(\text{SiO}_4)_4(\text{PO}_4)_2\text{O}_2$ [17], $\text{Na}_4\text{CaSi}_3\text{O}_9$ [18], Zn_2GeO_4 [19], $\text{Gd}_2\text{Zr}_2\text{O}_7$ [13], $\text{Sr}_3\text{YNa}(\text{PO}_4)_3\text{F}$ [20], LaVO_4 [21], *etc.* Within the field of luminous materials, research and technological advancement have been driven by search for new luminescent compounds exhibiting improved optical characteristics. So selecting an adequate host material is extremely essential for the phosphors featuring the spectacular illuminating character traits. In juxtaposed with silicates, fluorides, oxides, nitride, vanadates, oxynitride, sulfides, *etc.* aluminates have been revealed to be a more favourable host choice.

Rare earth elements have been incorporated into aluminate matrices to significantly alter the characteristics enabling an array of advanced applications. Due to their exceptional stability, elevated brightness, enduring after-glow, superior efficiency, and appropriate emission color, rare earth-doped aluminates have been the subject of intense research in recent years as ideal luminescent materials used in lighting and display technologies, as well as for usage in lasers, LEDs, and other photonic devices. The synthesis and structural composition of rare-earth enriched melilite families have been the subject of numerous investigation. In present investigation, $\text{LaSrAl}_3\text{O}_7$, a type of aluminates was chosen as the substrate matrix. This is one of the convoluted oxides in the huge group of rare-earth strontium aluminate with melilite structure. In literature, photoluminescence studies of $\text{LaSrAl}_3\text{O}_7$: Eu^{3+} , $\text{LaSrAl}_3\text{O}_7$: Tb^{3+} doped phosphors synthesised *via* solution combustion method [22], $\text{LaSrAl}_3\text{O}_7$: RE^{3+} (RE = Eu, Tb) phosphors prepared using sol gel method [23] and $\text{LaSrAl}_3\text{O}_7$: 0.01Eu^{3+} , $x\text{M}^+$ (M = K, Na, Li)

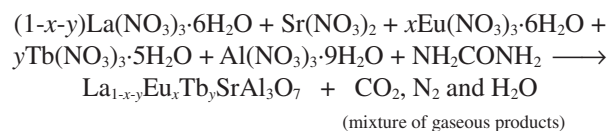
[24] phosphors obtained by solution combustion method and $\text{LaSrAl}_3\text{O}_7$: Eu^{3+} synthesized *via* solid-state reaction method [25] have been reported. However, the possible energy transfer process and influences of Eu^{3+} , Tb^{3+} co-doping in $\text{LaSrAl}_3\text{O}_7$ photoluminescence properties have not been reported in the literature till date.

In this work, $\text{La}_{0.99}\text{Eu}_{0.01}\text{SrAl}_3\text{O}_7$, $\text{La}_{0.99}\text{Tb}_{0.01}\text{SrAl}_3\text{O}_7$ and a series of $\text{La}_{0.99-x}\text{Eu}_x\text{Tb}_{0.01}\text{SrAl}_3\text{O}_7$ ($x = 0.01-0.07$ mol) co-doped nanocrystalline phosphor were prepared *via* simple, single step, self-propagating solution combustion method. The structural, morphological, band gap, luminescence and color-tunable characteristics were studied. Energy transfer from Tb^{3+} to Eu^{3+} ions in the host matrix was found to be effective simply adjusting the ratio of $\text{Eu}^{3+}/\text{Tb}^{3+}$ ions. Pursuant to the outcomes, the synthesized $\text{La}_{0.99-x}\text{Eu}_x\text{Tb}_{0.01}\text{SrAl}_3\text{O}_7$ ($x = 0.01-0.07$ mol) nanocrystalline luminescent materials showed emissions that could be adjusted from greenish to orange-red to a deep red. Consequently, it becomes realistic that $\text{Eu}^{3+}/\text{Tb}^{3+}$ co-doped $\text{LaSrAl}_3\text{O}_7$ can potentially be utilized as an effective illumination material in field emission displays, various light sources, photonic devices, pc-LEDs, full-color displays and other lighting fixtures.

EXPERIMENTAL

Synthesis of $\text{Eu}^{3+}/\text{Tb}^{3+}$ co-doped $\text{LaSrAl}_3\text{O}_7$ crystalline nanophosphors: An affordable, simple and self-propagating, urea-assisted solution combustion synthesis method was adopted in order to synthesize $\text{La}_{0.99}\text{Eu}_{0.01}\text{SrAl}_3\text{O}_7$, $\text{La}_{0.99}\text{Tb}_{0.01}\text{SrAl}_3\text{O}_7$ and a series of $\text{La}_{0.99-x}\text{Eu}_x\text{Tb}_{0.01}\text{SrAl}_3\text{O}_7$, co-doped phosphors where $x = 0.01-0.07$ mol. For combustion, the raw ingredients (metal nitrates) of high-purity *i.e.* $\text{La}(\text{NO}_3)_3 \cdot 6\text{H}_2\text{O}$, $\text{Eu}(\text{NO}_3)_3 \cdot 6\text{H}_2\text{O}$, $\text{Sr}(\text{NO}_3)_2$, $\text{Al}(\text{NO}_3)_3 \cdot 9\text{H}_2\text{O}$, $\text{Tb}(\text{NO}_3)_3 \cdot 5\text{H}_2\text{O}$ as oxidants and urea (NH_2CONH_2) as fuel were used. Despite the aid of another heating origin, the process could be rapidly accelerated to extremely elevated temperatures *via* the energy produced by the exothermic process that occurs amid the metal nitrates and urea (fuel). Indeed, the combustion process facilitates the quick fabrication of plenty of inorganic materials sans the need for the lengthy, high-temperature sintering step [11,26-28]. In a stoichiometric ratio, the starting ingredients (metal nitrates + fuel) were dissolved with minimum quantity of deionized water in a beaker. The resulting solution was subsequently heated on a hot plate with dynamic stirring for a maximum of two to three min to achieve a homogeneous mixture. The homogeneous solution was then inserted in a muffle furnace maintained at 500°C for heating for 4-6 min. A robust exothermic process results in the emergence of combustible gasses and that yields a fluffy voluminous solid material [22,24, 26,29].

The basic chemical route which prompted doped/co-doped $\text{La}_{1-x-y}\text{Eu}_x\text{Tb}_y\text{SrAl}_3\text{O}_7$ crystalline phosphor was delineated as follows:



Here ($x = 0$, $y = 0.01$ mol), ($x = 0.01$ mol, $y = 0$) and ($x = 0.01-0.07$ mol, $y = 0.01$ mol). After cooling the obtained volum-

inous substances to room temperature, an agate mortar was used for grinding them into powder. Following that, the uniform powders were placed in a crucible and annealed at 900 °C for 3 h, yielding the required crystalline material and preserved in a desiccator for further analysis [30].

Characterization of La_{1-x-y}Eu_xTb_ySrAl₃O₇ co-doped nanocrystalline phosphors: The crystallographic phase analysis of the synthesized Eu³⁺/Tb³⁺ co-doped LaSrAl₃O₇ nanomaterials were evaluated by engaging Rigaku Ultima IV X-ray powder diffractometer with Ni-filtered CuK_α radiations with $\lambda = 0.154056$ nm. The field emission scanning electron microscopy (FE-SEM) imaging as well as transmission electron microscopy (TEM) was employed for assessing the surface appearance and particle size of the produced co-doped phosphors. The precise elemental composition of the synthesized phosphors was determined with energy dispersive X-ray analysis (EDAX). Using BaSO₄ as a reference compound, Shimadzu UV-3600 plus UV-Vis-NIR spectrophotometer was used to analyze the energy band gap of the synthesized co-doped nanophosphor. A HORIBA fluorescence spectrophotometer with a xenon lamp was used to perform the photoluminescence analysis. Commission International de l'Eclairage 1931 (CIE) color coordinates (x, y) and other important photometric properties of the produced La_{1-x-y}Eu_xTb_ySrAl₃O₇ nanocrystalline luminescent samples were also determined from the exploration of their photoluminescent data. All the above mentioned characterizations were carried out at room temperature.

RESULTS AND DISCUSSION

XRD studies: The phase consistency and structural features of co-doped crystalline La_{0.95}Eu_{0.04}Tb_{0.01}SrAl₃O₇ nanophosphor was studied by analyzing its diffraction pattern as shown in Fig. 1. The frameworks of LaSrAl₃O₇ compounds were composed of 5-membered rings constructed with AlO₄⁵⁻ tetrahedral, Sr²⁺ and La³⁺ ions appear sporadically dispersed in eight coordinating positions with Cs symmetry between the layers [22]. Precise peaks in the XRD image (Fig. 1) effectively harmonized with the standard JCPDS card no. 50-1815, which revealed the formation of crystalline and pure single phase La_{0.95}Eu_{0.04}Tb_{0.01}SrAl₃O₇ co-doped phosphor at 900 °C. In contrast to the solid-state reaction synthesis approach, the sintering temperature has been dropped to approximately 500 °C [25,29]. The diffraction peaks of Eu³⁺/Tb³⁺ co-doped LaSrAl₃O₇ sintered at 900 °C (3 h) primarily belong to tetragonal crystalline structure with space group of *P42₁m* (113). It was evident that the nanophosphor had been successfully produced in a single phase at this temperature as no spike patterns attributable to additional phases could be spotted [23,24]. Furthermore, the lack of extra peaks in the diffraction pattern within the 10-80° scanning range demonstrated that the co-doping of Eu³⁺/Tb³⁺ ions within the lattice matrix did not influence LaSrAl₃O₇ basic framework [12,31].

The dopant ions (Eu³⁺ and Tb³⁺) assumed to have substituted lanthanum (La³⁺) ions in the LaSrAl₃O₇ host lattice in lieu of other (aluminum and strontium) ions because of their nearly comparable sizes and charges. The difference in percentage (%) radius (D_r) was derived in order to gain a better under-

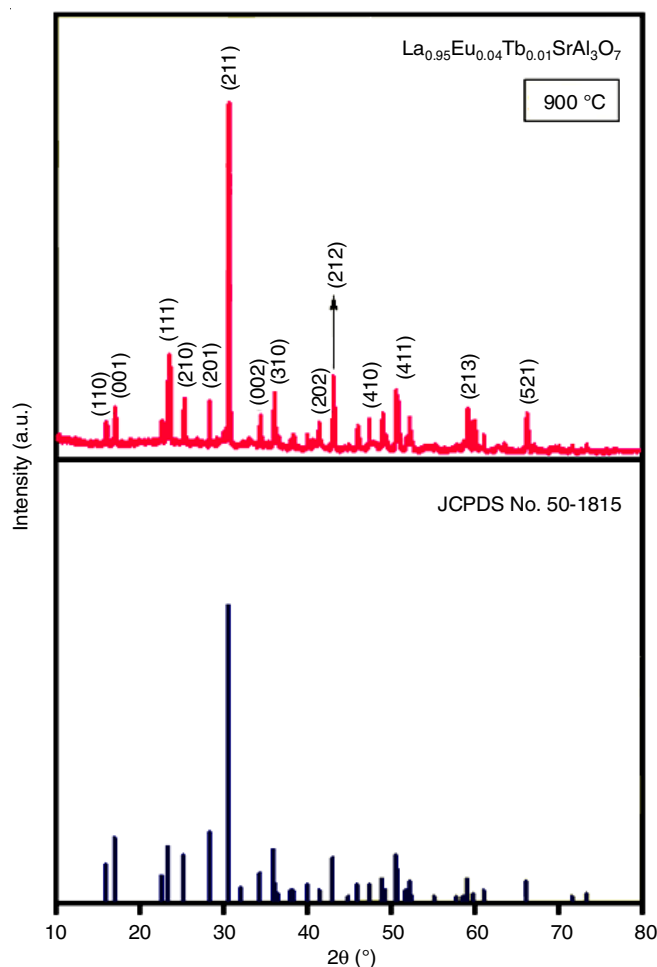


Fig. 1. XRD patterns of La_{0.95}Eu_{0.04}Tb_{0.01}SrAl₃O₇ phosphor sintered at 900 °C with standard data for LaSrAl₃O₇ (JCPDS No. 50-1815)

standing of the substitution phenomenon in LaSrAl₃O₇ matrix by dopant ions (Eu³⁺ and Tb³⁺). For the formation of an adequate crystal lattice, D_r should have a value of less than 30% [32,33]. The equation used in this instance was as follows:

$$D_r (\%) = \frac{R_h (\text{CN}) - R_d (\text{CN})}{R_h (\text{CN})} \times 100 \quad (1)$$

The respective ionic radii of the host and doping ions, designated by the initials R_h and R_d as well as the coordination number, represented by CN in eqn 1. Considering all of the values, D_r (%) for the combos of La³⁺/Tb³⁺ and La³⁺/Eu³⁺ was determined to be 9.53% and 16%, respectively [34,35]. Privileged substitution seems generally supported to require a radius variation of less than 30% among the infused ions and host ions. It culminates in the preferential substitution of Eu³⁺/Tb³⁺ ions for lanthanum ions in LaSrAl₃O₇ host lattice as obtained through utilizing eqn 1.

The nanocrystalline nature of La_{0.95}Eu_{0.04}Tb_{0.01}SrAl₃O₇ co-doped powder sintered at 900 °C for 3 h was assessed from the average size of crystallite (D), which was obtained using Scherrer's formula (eqn. 2) [4,13,36].

$$D = \frac{0.941\lambda}{\beta \cos \theta} \quad (2)$$

where D = average grain size; λ = X-rays wavelength of $\text{CuK}\alpha$ radiation (0.154056 nm); θ = Bragg's angle of an observed X-ray diffraction peak; β = Full width at half-maxima in radians (FWHM).

From Scherrer's formula, the average grain size was found to be 37.55 nm. The Williamson-Hall (W-H) relation, which validates Scherrer's approach, was also used to determine the average crystallite size of $\text{La}_{0.95}\text{Eu}_{0.04}\text{Tb}_{0.01}\text{SrAl}_3\text{O}_7$ co-doped nanocrystalline phosphor sintered at 900 °C, along with other crystallographic data including microstrain (ϵ) and dislocation density (δ) [37-40] as follows:

$$\beta \cos \theta = \epsilon(4 \sin \theta) + \frac{0.89\lambda}{D} \quad (3)$$

$$\text{Dislocation density } (\delta) = \frac{1}{D^2} \quad (4)$$

The correlation inferred by eqn. 3 between $\beta \cos \theta$ and $4 \sin \theta$ has culminated in a straight line graph. The value of the straight-line intercept corresponds to the average crystallite size (D). The microstrain value was subsequently derived from the slope of line. The strain value of 0.00208 and the crystalline size value of 63.60 nm have been retrieved from the W-H plot (Fig. 2) using the slope and Y-intercept of fit, respectively. The grain size value derived by the W-H approach was found to be marginally larger than the value derived from Scherrer's equation because strain considered in the W-H approach not in Scherrer's approach [41,42]. Also, dislocation density ($\delta = 0.000247 \text{ nm}^{-2}$) has been determined using eqn. 4. A comprehensive investigation of both phase analysis and crystallographic aspects disclosed the formation of single phase $\text{Eu}^{3+}/\text{Tb}^{3+}$ co-doped $\text{LaSrAl}_3\text{O}_7$ crystalline nanophosphors.

Morphological studies: The tailored $\text{Eu}^{3+}/\text{Tb}^{3+}$ co-doped $\text{LaSrAl}_3\text{O}_7$ sample surface morphology, nanostructure and $\text{Eu}^{3+}/\text{Tb}^{3+}$ ions distributions were studied through FE-SEM, TEM and EDAX techniques. The optimized $\text{La}_{0.95}\text{Eu}_{0.04}\text{Tb}_{0.01}\text{SrAl}_3\text{O}_7$ phosphor sample sintered at 900 °C revealed agglomerates featuring spherical-shaped porous particles having discrete inter-

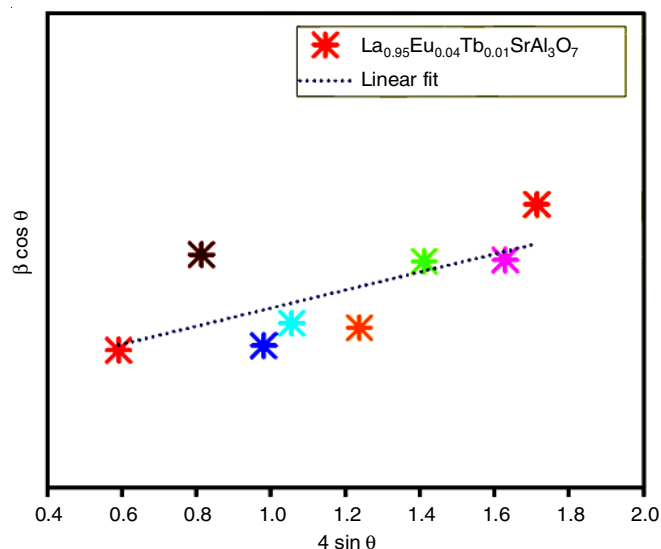


Fig. 2. W-H plot of $\text{La}_{0.95}\text{Eu}_{0.04}\text{Tb}_{0.01}\text{SrAl}_3\text{O}_7$ nanophosphor sintered at 900 °C

connect boundaries and smooth surface as demonstrated in the FE-SEM image (Fig. 3a). The FE-SEM image clearly exhibited some small pores as a consequence of the release of volatile by-products. Such physical features enable to recognize particles, which have been produced as the consequence of solution combustion synthesis method [43-45].

The large surface area was developed by the densely packed, sharing margins of the particles safeguards it from aging. The effectiveness of luminescence of nanophosphor is boosted owing to its smooth surface influence, which minimizes non-radiation and scattering [22,46,47]. Fig. 3b illustrated the TEM image of annealed $\text{La}_{0.95}\text{Eu}_{0.04}\text{Tb}_{0.01}\text{SrAl}_3\text{O}_7$ phosphor at 900 °C and indicated the loosely organized bunches of spherical shaped nano-scale particles [22]. Fig. 4 exhibits the EDAX mappings for all relevant constituents. The resulting maps reflect substantial loading of $\text{Eu}^{3+}/\text{Tb}^{3+}$ within $\text{LaSrAl}_3\text{O}_7$ substrate lattice, as well as the fair deployment of the distinct ingredients. The EDAX spectrum (Fig. 5) shows the spikes that correspond to the

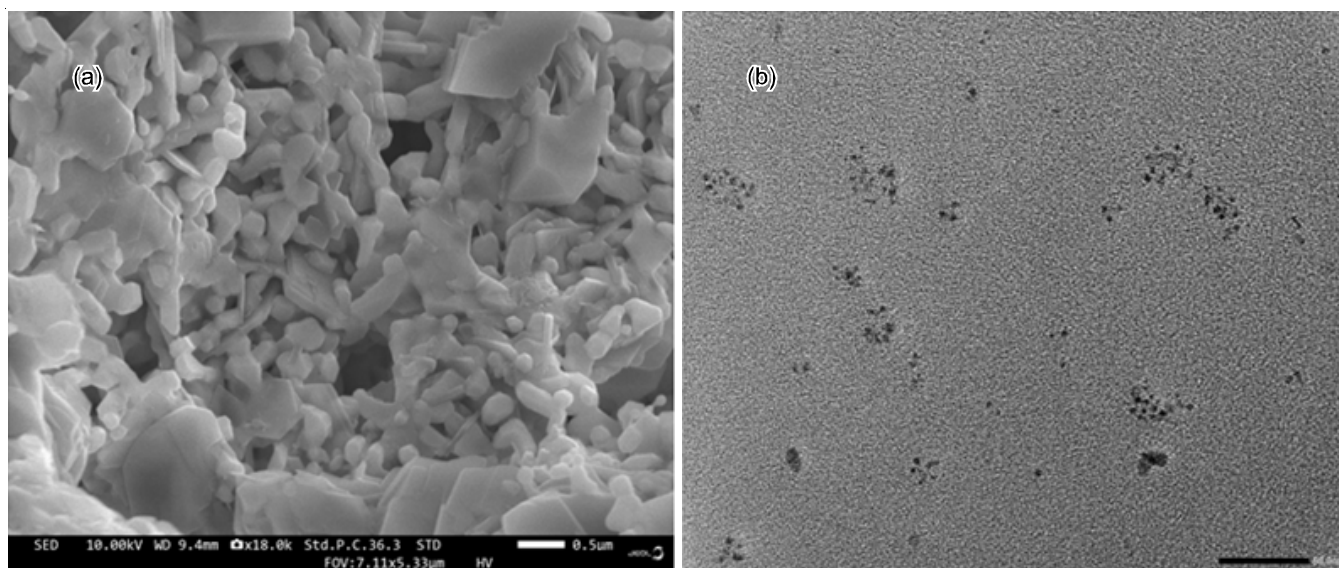


Fig. 3. (a) FE-SEM image and (b) TEM image of $\text{La}_{0.95}\text{Eu}_{0.04}\text{Tb}_{0.01}\text{SrAl}_3\text{O}_7$ nanophosphor synthesized *via* solution combustion method

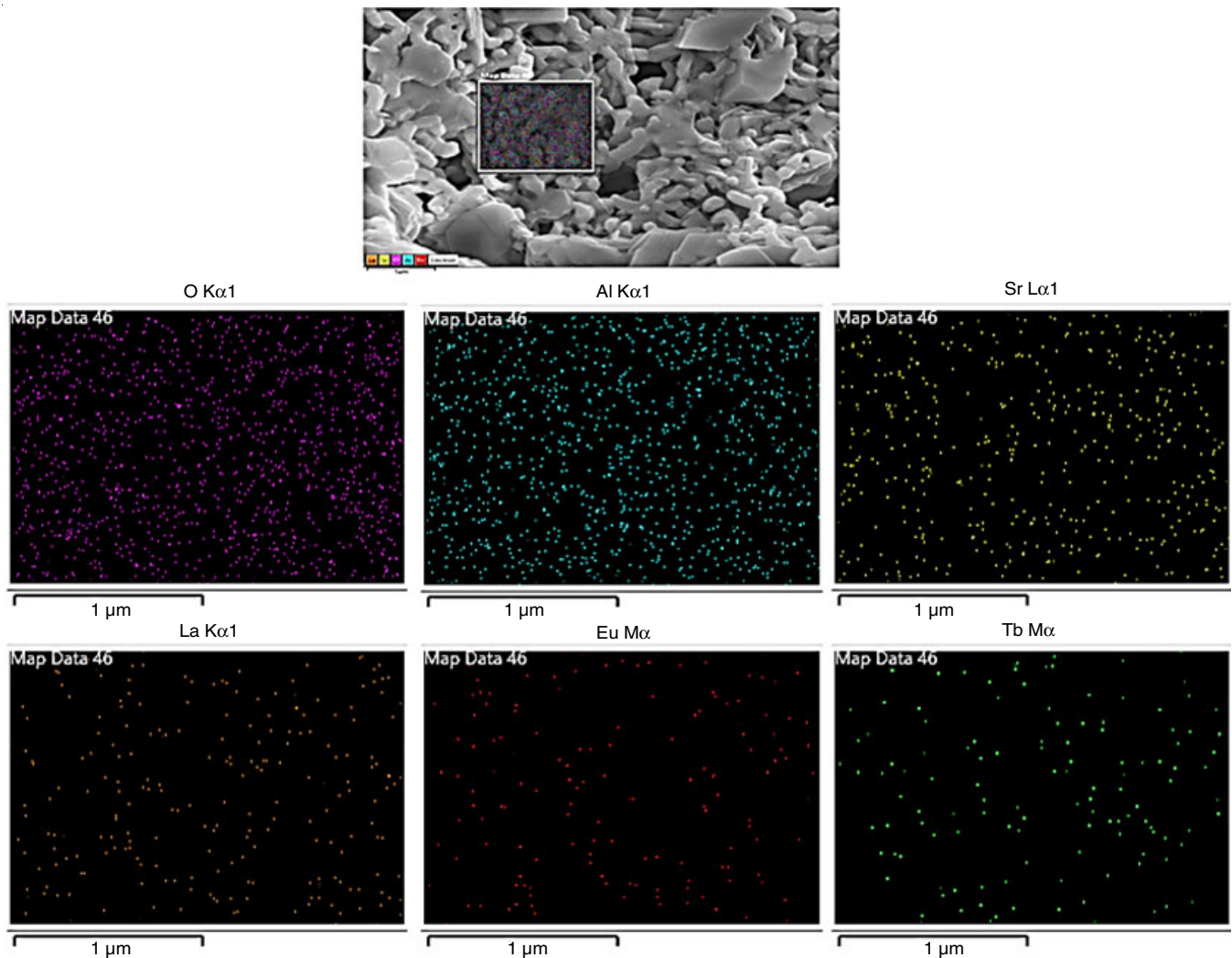


Fig. 4. EDAX spectra portraying elemental mapping of La_{0.95}Eu_{0.04}Tb_{0.01}SrAl₃O₇ nanophosphor sintered at 900 °C

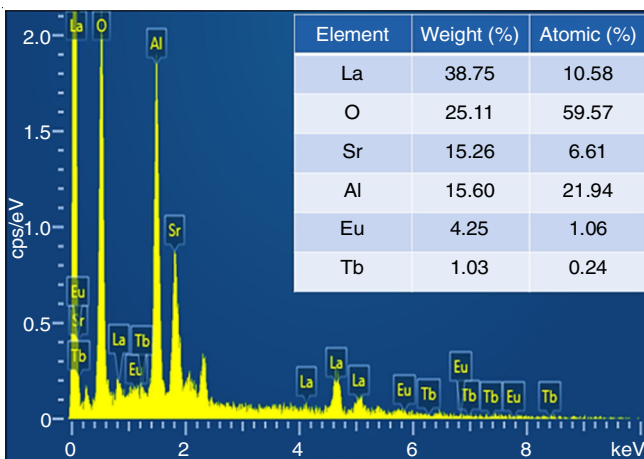


Fig. 5. EDAX spectra of co-doped La_{0.95}Eu_{0.04}Tb_{0.01}SrAl₃O₇ nanophosphor sintered at 900 °C

constituent ingredients (Tb, Eu, La, Sr, Al and O). The atomic percentage and weight percentages compositions of each component were also included as an inset [25,48]. All investigations indicated that the resulting strontium aluminum lanthanum oxide samples doped efficiently with Eu³⁺ and Tb³⁺ ions.

Optical band gap studies: The optical properties of the La_{0.99}Eu_{0.01}SrAl₃O₇, La_{0.99}Tb_{0.01}SrAl₃O₇ and La_{0.99-x}Eu_xTb_{0.01}SrAl₃O₇, co-doped phosphors where ($x = 0.01-0.07$ mol) were probed through diffuse reflectance (DR) spectroscopy. It serves as a forefront way of assessing the spectroscopic traits of solid materials, including powder or thin films. The diffuse reflectance patterns and calculated band gap values for synthesized co-doped luminescent materials are shown in Figs. 6 and 7, respectively. The La_{0.99-x}Eu_xTb_{0.01}SrAl₃O₇ ($x = 0.01-0.07$ mol) luminescent nanomaterials demonstrated energy absorption in < 300 nm domain, which was analogous to photoluminescent excitation spectrum. In region ≤ 300 nm, La_{0.99-x}Eu_xTb_{0.01}SrAl₃O₇ ($x = 0.01-0.07$ mol) luminescent materials showed energy absorption at 255 nm corresponding to charge transfer from O²⁻ to Eu³⁺. The minor absorption bands in > 300 nm region (Fig. 6) correlated with the 4*f* intra-configurational transitions of Eu³⁺ and Tb³⁺ ions [13,49,50]. The Kubelka-Munk function (eqn. 5) and Tauc's relation (eqn. 6) were utilized to assess the probe concurrent to the DR spectra, *i.e.* the determination of optical band gap of La_{0.99}Eu_{0.01}SrAl₃O₇, La_{0.99-x}Eu_xTb_{0.01}SrAl₃O₇ ($x = 0.01-0.07$ mol) and La_{0.99}Tb_{0.01}SrAl₃O₇ nanocrystalline materials [51-56].

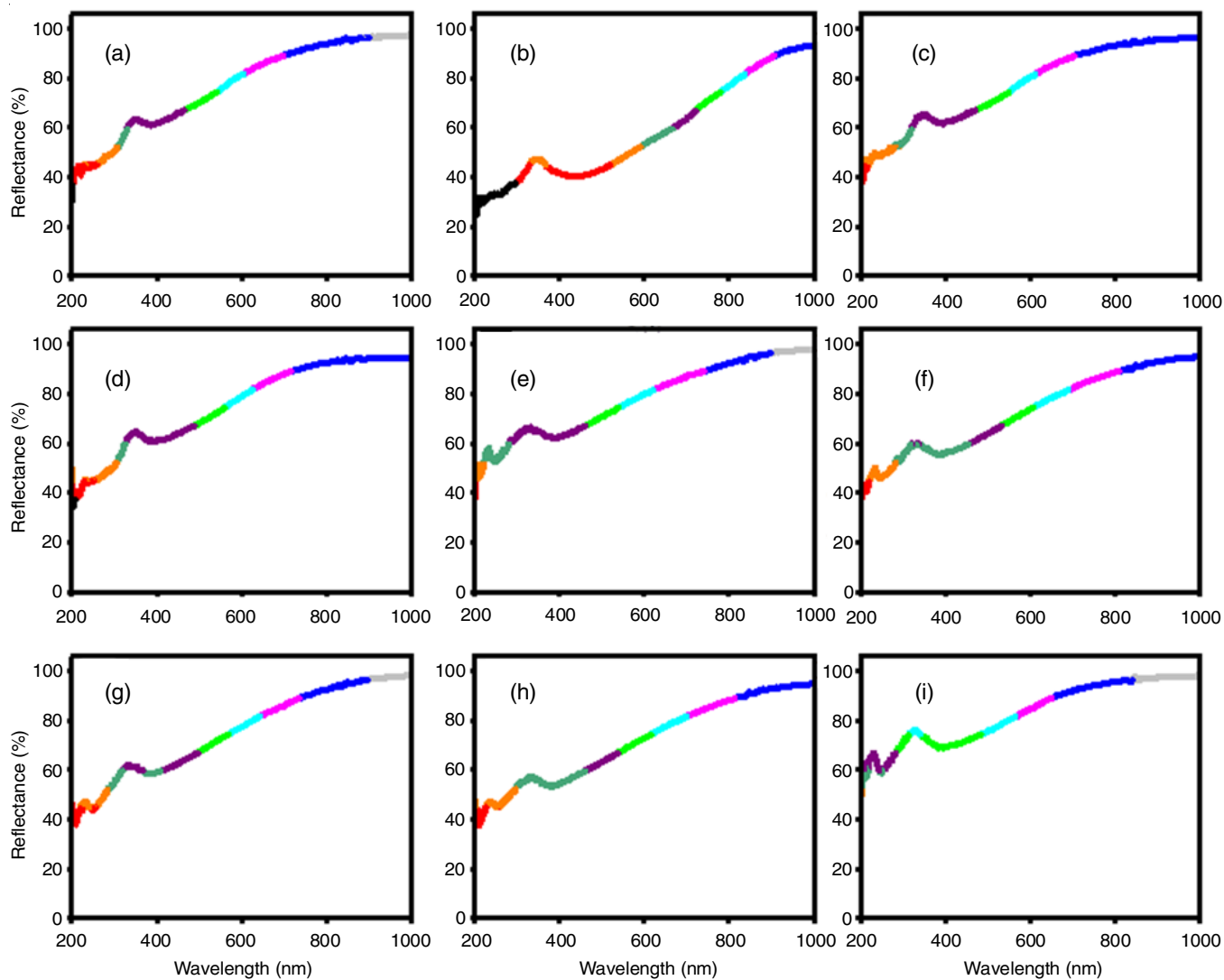


Fig. 6. Diffuse reflectance spectra of (a) $\text{La}_{0.99}\text{Eu}_{0.01}\text{SrAl}_3\text{O}_7$, (b-h) $\text{La}_{0.99-x}\text{Eu}_x\text{Tb}_{0.01}\text{SrAl}_3\text{O}_7$ ($x = 0.01-0.07$ mol) and (i) $\text{La}_{0.99}\text{Tb}_{0.01}\text{SrAl}_3\text{O}_7$ phosphors

$$F(R_\infty) = \frac{(1 - R_\infty)^2}{2R_\infty} = \frac{K}{S} \quad (5)$$

$$[F(R_\infty) h\nu]^n = C(h\nu - E_g) \quad (6)$$

where $F(R_\infty)$ = Kubelka-Munk function; $h\nu = 1240/\lambda$ R = sample reflection coefficient; C = proportionality constant; K = absor-

ption coefficient; S = scattering coefficient; and n = electronic transition nature (n = 1/2, direct allowed transitions, n = 2, indirect allowed transitions, n = 3, indirect forbidden transitions and n = 3/2, direct forbidden transitions, respectively).

The optimal band gap (E_g) of all the these phosphors were calculated [36,57] and the values are tabulated in Table-1. With regard to Eu^{3+} and Tb^{3+} mono-doped $\text{LaSrAl}_3\text{O}_7$ phosphors, the

TABLE-1
ENERGY BAND GAP (eV), REFRACTIVE INDEX (n) AND METALLIZATION CRITERION (M) OF
 $\text{La}_{0.99}\text{Eu}_{0.01}\text{SrAl}_3\text{O}_7$, $\text{La}_{0.99-x}\text{Eu}_x\text{Tb}_{0.01}\text{SrAl}_3\text{O}_7$ ($x = 0.01-0.07$ mol) AND $\text{La}_{0.99}\text{Tb}_{0.01}\text{SrAl}_3\text{O}_7$ NANOMATERIALS

Symbolization	Phosphor sample	Energy band gap (eV)	Refractive index (n)	Metallization criterion (M)
a	$\text{La}_{0.99}\text{Eu}_{0.01}\text{SrAl}_3\text{O}_7$	4.00	2.17	0.447
b	$\text{La}_{0.98}\text{Eu}_{0.01}\text{Tb}_{0.01}\text{SrAl}_3\text{O}_7$	4.23	2.12	0.459
c	$\text{La}_{0.97}\text{Eu}_{0.02}\text{Tb}_{0.01}\text{SrAl}_3\text{O}_7$	4.49	2.08	0.474
d	$\text{La}_{0.96}\text{Eu}_{0.03}\text{Tb}_{0.01}\text{SrAl}_3\text{O}_7$	4.65	2.05	0.482
e	$\text{La}_{0.95}\text{Eu}_{0.04}\text{Tb}_{0.01}\text{SrAl}_3\text{O}_7$	4.74	2.04	0.486
f	$\text{La}_{0.94}\text{Eu}_{0.05}\text{Tb}_{0.01}\text{SrAl}_3\text{O}_7$	4.78	2.03	0.488
g	$\text{La}_{0.93}\text{Eu}_{0.06}\text{Tb}_{0.01}\text{SrAl}_3\text{O}_7$	5.25	1.96	0.512
h	$\text{La}_{0.92}\text{Eu}_{0.07}\text{Tb}_{0.01}\text{SrAl}_3\text{O}_7$	4.89	2.01	0.494
i	$\text{La}_{0.99}\text{Tb}_{0.01}\text{SrAl}_3\text{O}_7$	3.92	2.19	0.443

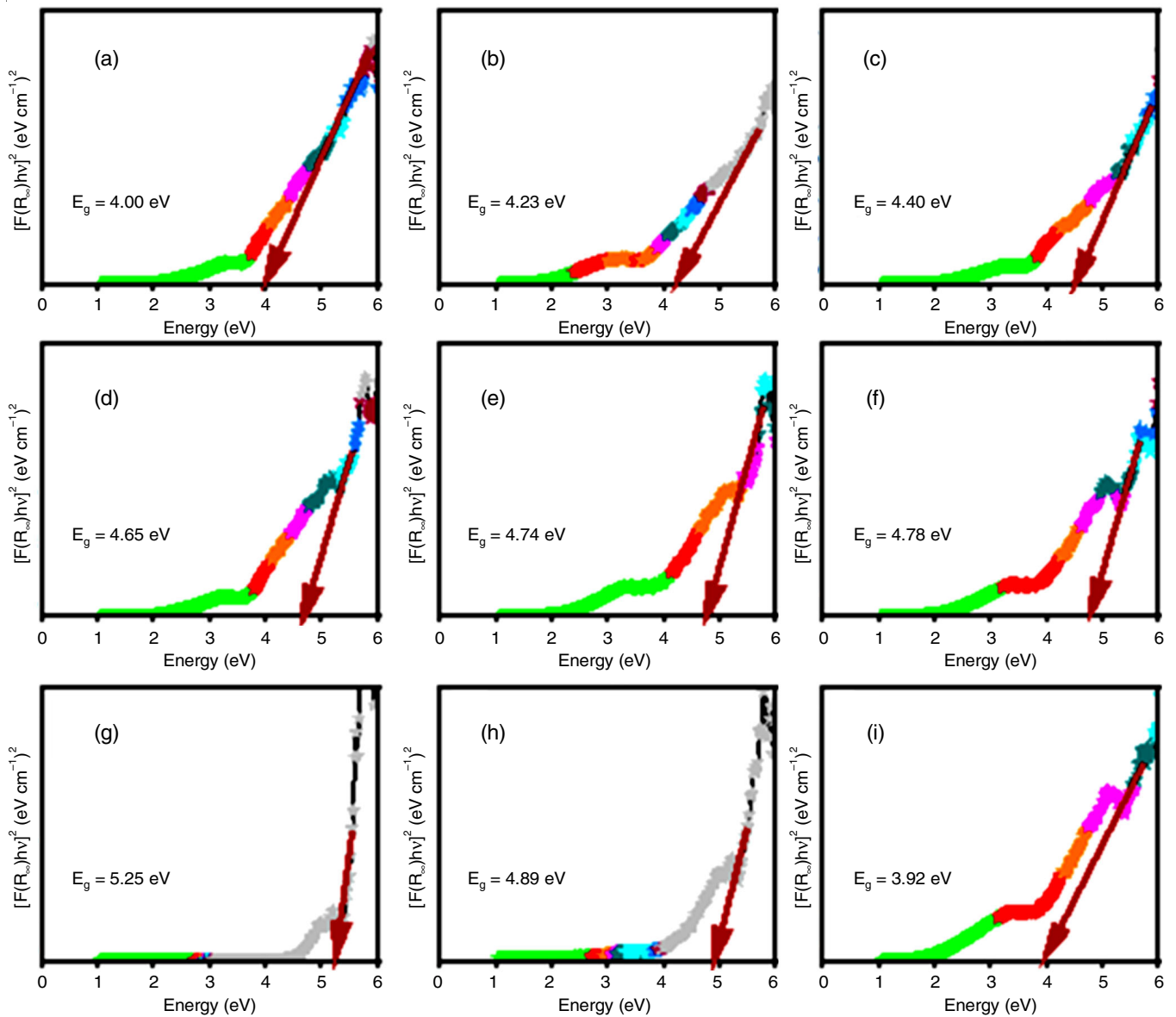


Fig. 7. Optimal band gap (E_g) of (a) La_{0.99}Eu_{0.01}SrAl₃O₇, (b-h) La_{0.99-x}Eu_xTb_{0.01}SrAl₃O₇ ($x = 0.01 - 0.07$ mol) and (i) La_{0.99}Tb_{0.01}SrAl₃O₇ phosphors

fluctuation in the E_g value of Eu³⁺/Tb³⁺ co-doped LaSrAl₃O₇ nanomaterial reveals the accumulation of a few additional levels of energy of doped ions. As the concentration of Eu³⁺ ions increased, it was observed that the E_g of La_{0.99-x}Eu_xTb_{0.01}SrAl₃O₇ nanophosphors widens attributable to the Moss effect. However, if Eu³⁺ ions concentration rises further, the energy band gap shrinks, this could be due to dopant ion sublevels emerging proximal to the conduction band [49,58-62]. Also, the energy band gap values of La_{0.99}Eu_{0.01}SrAl₃O₇, La_{0.99-x}Eu_xTb_{0.01}SrAl₃O₇ ($x = 0.01 - 0.07$ mol) and La_{0.99}Tb_{0.01}SrAl₃O₇ phosphors materials were used in eqns. 7 and 8 to determine the refractive index (n) and metallization criterion (M) of these synthesized materials.

$$\frac{n^2 - 1}{n^2 + 2} = 1 - \sqrt{\frac{E_g}{20}} \quad (7)$$

$$M = 1 - \frac{n^2 - 1}{n^2 + 2} = \sqrt{\frac{E_g}{20}} \quad (8)$$

The theoretically calculated metallization criterion ($M < 1$) by Dimitrov and Sakka's expression (eqn. 8) validating the non-metallic character of co-doped La_{0.99-x}Eu_xTb_{0.01}SrAl₃O₇ ($x = 0.01 - 0.07$ mol) nanosamples [58,63,64].

Luminescence studies: The photoluminescence excitation (PLE) and photoluminescence emission (PL) spectra of La_{0.99}Eu_{0.01}SrAl₃O₇ observed at 617 nm and 255 nm, respectively are shown in Fig. 8. The PLE spectrum of doped La_{0.99}Eu_{0.01}SrAl₃O₇ nanophosphor monitored at $\lambda_{em} = 617$ nm corresponding to the ⁵D₀ → ⁷F₂ transition (Eu³⁺) shown in Fig. 8(left) exhibited five excitations bands due to the charge transfer band (CTB) of O²⁻-Eu³⁺ bond (255 nm), ⁷F₀ → ⁵H₅ (321 nm), ⁷F₀ → ⁵D₄ (360 nm), ⁷F₀ → ⁵L₆ (392 nm) and ⁷F₀ → ⁵D₂ (464 nm) transitions [23,65,66]. The emission spectrum of La_{0.99}Eu_{0.01}SrAl₃O₇ phosphor monitoring at $\lambda_{ex} = 255$ nm exhibited emission bands corresponding to ⁵D₀ → ⁷F₁ (589 nm), ⁵D₀ → ⁷F₂ (612, 617 nm) and ⁵D₀ → ⁷F₃ (655 nm) transitions (Table-2). The emission spectra revealed non-centrosymmetric arrangement of Eu³⁺ ions in

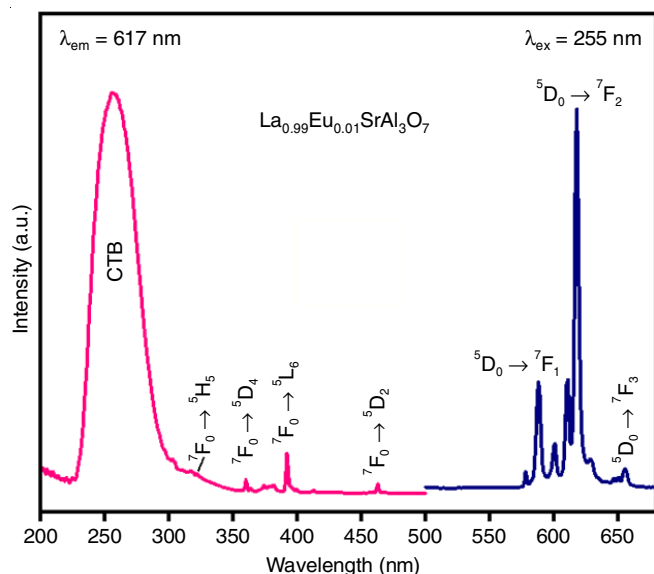


Fig. 8. PLE and PL spectra of $\text{La}_{0.99}\text{Eu}_{0.01}\text{SrAl}_3\text{O}_7$ nanocrystalline phosphor sintered at 900 °C

TABLE-2 PL EXCITATION, EMISSION PEAKS AND CORRELATIVE TRANSITION DELINEATE OF $\text{La}_{0.99}\text{Eu}_{0.01}\text{SrAl}_3\text{O}_7$, $\text{La}_{0.99}\text{Tb}_{0.01}\text{SrAl}_3\text{O}_7$, AND $\text{La}_{0.99-x}\text{Eu}_x\text{Tb}_{0.01}\text{SrAl}_3\text{O}_7$ NANOPHOSPHORS			
Transitions	λ_{ex} (nm)	Transitions	λ_{em} (nm)
$\text{La}_{0.99}\text{Eu}_{0.01}\text{SrAl}_3\text{O}_7$ nanophosphor			
CTB	255	$^5\text{D}_0 \rightarrow ^7\text{F}_1$	589
$^7\text{F}_0 \rightarrow ^5\text{H}_5$	321	$^5\text{D}_0 \rightarrow ^7\text{F}_2$	612, 617
$^7\text{F}_0 \rightarrow ^5\text{D}_4$	360	$^5\text{D}_0 \rightarrow ^7\text{F}_3$	655
$^7\text{F}_0 \rightarrow ^5\text{L}_6$	392		
$^7\text{F}_0 \rightarrow ^5\text{D}_2$	464		
$\text{La}_{0.99}\text{Tb}_{0.01}\text{SrAl}_3\text{O}_7$ nanophosphor			
$4f^8 \rightarrow 4f^7 5d^1$	235	$^5\text{D}_3 \rightarrow ^7\text{F}_5$	415
$^7\text{F}_6 \rightarrow ^5\text{D}_1$	318	$^5\text{D}_3 \rightarrow ^7\text{F}_4$	439
$^7\text{F}_6 \rightarrow ^5\text{G}_2$	339	$^5\text{D}_4 \rightarrow ^7\text{F}_6$	485
$^7\text{F}_6 \rightarrow ^5\text{D}_3$	366	$^5\text{D}_4 \rightarrow ^7\text{F}_5$	544
$^7\text{F}_6 \rightarrow ^5\text{L}_{10}$	376	$^5\text{D}_4 \rightarrow ^7\text{F}_4$	593
		$^5\text{D}_4 \rightarrow ^7\text{F}_3$	622
$\text{La}_{0.99-x}\text{Eu}_x\text{Tb}_{0.01}\text{SrAl}_3\text{O}_7$ ($x = 0.01-0.07$ mol) nanophosphors			
CTB	255	$^5\text{D}_4 \rightarrow ^7\text{F}_5$	544
$^7\text{F}_0 \rightarrow ^5\text{H}_5$	321	$^5\text{D}_0 \rightarrow ^7\text{F}_1$	589
$^7\text{F}_0 \rightarrow ^5\text{D}_4$	360	$^5\text{D}_0 \rightarrow ^7\text{F}_2$	612, 617
$^7\text{F}_0 \rightarrow ^5\text{L}_6$	392	$^5\text{D}_0 \rightarrow ^7\text{F}_3$	655
$^7\text{F}_0 \rightarrow ^5\text{D}_2$	464		

λ_{ex} = Excitation wavelength, λ_{em} = Emission wavelength, CTB = Charge transfer band

$\text{LaSrAl}_3\text{O}_7$ host lattice as evident by much greater red-light emission intensity corresponding to the electric dipole transition ($^5\text{D}_0 \rightarrow ^7\text{F}_2$) than the orange-red emission corresponding to the magnetic dipole transition ($^5\text{D}_0 \rightarrow ^7\text{F}_1$) [22,67-69].

The PLE spectrum (Fig. 9) of $\text{La}_{0.99}\text{Tb}_{0.01}\text{SrAl}_3\text{O}_7$ phosphor nanosample monitored at $\lambda_{\text{em}} = 544$ nm, exhibited a prominent band 235 nm generated from spin-permitted $4f^8 \rightarrow 4f^7 5d^1$ transition and some other bands at 318 ($^7\text{F}_6 \rightarrow ^5\text{D}_1$), 339 ($^7\text{F}_6 \rightarrow ^5\text{G}_2$), 366 ($^7\text{F}_6 \rightarrow ^5\text{D}_3$) and 376 ($^7\text{F}_6 \rightarrow ^5\text{L}_{10}$) that were attributed to $4f^8-4f^8$ intraconfigurational transitions of Tb^{3+} ion in $\text{LaSrAl}_3\text{O}_7$ host matrix. The emission spectrum

(Fig. 9, right) of $\text{La}_{0.99}\text{Tb}_{0.01}\text{SrAl}_3\text{O}_7$ nanophosphor monitored at $\lambda_{\text{ex}} = 235$ exhibited by the six emission bands in 400-650 nm region corresponding to $^5\text{D}_3 \rightarrow ^7\text{F}_5$ (415 nm), $^5\text{D}_3 \rightarrow ^7\text{F}_4$ (439 nm), $^5\text{D}_4 \rightarrow ^7\text{F}_6$ (485 nm), $^5\text{D}_4 \rightarrow ^7\text{F}_5$ (544 nm), $^5\text{D}_4 \rightarrow ^7\text{F}_4$ (593 nm) and $^5\text{D}_4 \rightarrow ^7\text{F}_3$ (622 nm) transitions of Tb^{3+} ions [15,22,70].

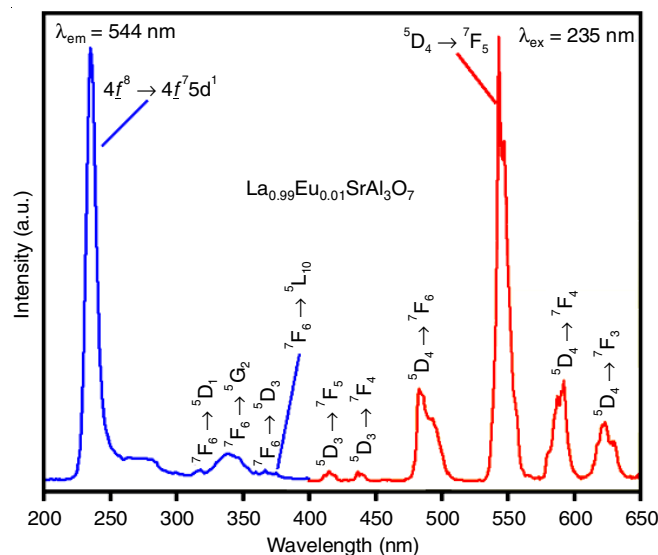


Fig. 9. PLE and PL spectra of $\text{La}_{0.99}\text{Tb}_{0.01}\text{SrAl}_3\text{O}_7$ nanocrystalline phosphor sintered at 900 °C

Additionally, there are numerous potentials of tunable light manifestations that may originate *via* the union of two or more trivalent lanthanides ions as dopants in a host system, comprising solid-state lighting, colored light emitting diodes, display devices etc. Emission lines typically distinctive features of specific rare earth ions. The mixing of different trivalent rare earth ions into the phosphors material will culminate in customizable luminous capabilities [54,71-73]. Pursuant to the Dexter theory, there needs to be a coincidence between the PL spectrum of Tb^{3+} ions and the PLE spectrum of Eu^{3+} ions for effective energy transfer. The preliminary desire for energy transfer has been fulfilled, as shown by Fig. 10, revealing that the PLE spectrum of Eu^{3+} ions and the PL spectrum of Tb^{3+} ions in $\text{LaSrAl}_3\text{O}_7$ matrix barely overlapped in 400-500 nm region [74,75]. The phonons spectrum could assist transfer of energy from $\text{Tb}^{3+} \rightarrow \text{Eu}^{3+}$, according to the literature evidence especially in scenarios if there is a slight spectral crossover. Thus, it could be concluded that energy transfer from $\text{Tb}^{3+} \rightarrow \text{Eu}^{3+}$ ions in selected lattice may occur in the context of co-doping of Tb^{3+} and Eu^{3+} ions [67,76,77].

For additional insight regarding the intriguing luminance aspects of $\text{La}_{0.99-x}\text{Eu}_x\text{Tb}_{0.01}\text{SrAl}_3\text{O}_7$ ($x = 0.01-0.07$ mol) nanocrystalline phosphor materials, the PLE and PL spectra of these co-doped nanophosphors were examined. The PLE and PL spectra of $\text{La}_{0.99-x}\text{Eu}_x\text{Tb}_{0.01}\text{SrAl}_3\text{O}_7$ ($x = 0.01-0.07$ mol) phosphors, obtained at monitoring $\lambda_{\text{em}} = 617$ and $\lambda_{\text{ex}} = 255$ nm depicted in Figs. 11 and 12, respectively. The combined PLE spectra of $\text{La}_{0.99-x}\text{Eu}_x\text{Tb}_{0.01}\text{SrAl}_3\text{O}_7$ ($x = 0.01-0.07$ mol) phosphors showed a striking resemblance to PLE spectrum of $\text{La}_{0.99}\text{Eu}_{0.01}\text{SrAl}_3\text{O}_7$ phosphor (Fig. 8). The excitation band attributed to Tb^{3+} ions appeared significantly overlaid by Eu^{3+} ions

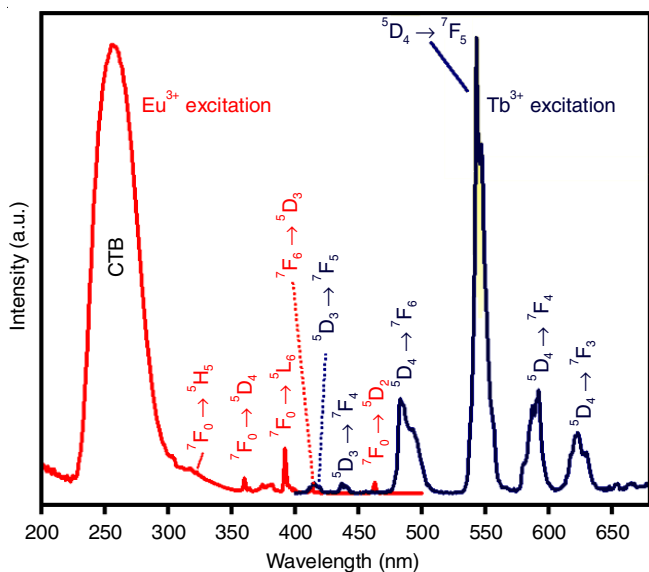


Fig. 10. Extent of spectral overlap among Eu³⁺ excitation and Tb³⁺ emission in LaSrAl₃O₇ matrix

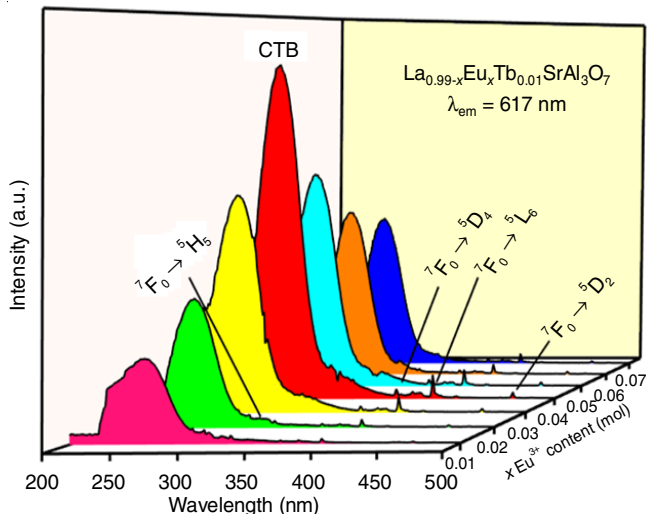


Fig. 11. Combined excitation spectra of La_{0.99-x}Eu_xTb_{0.01}SrAl₃O₇ ($x = 0.01-0.07$ mol) co-doped nanocrystalline phosphors at $\lambda_{em} = 617$ nm

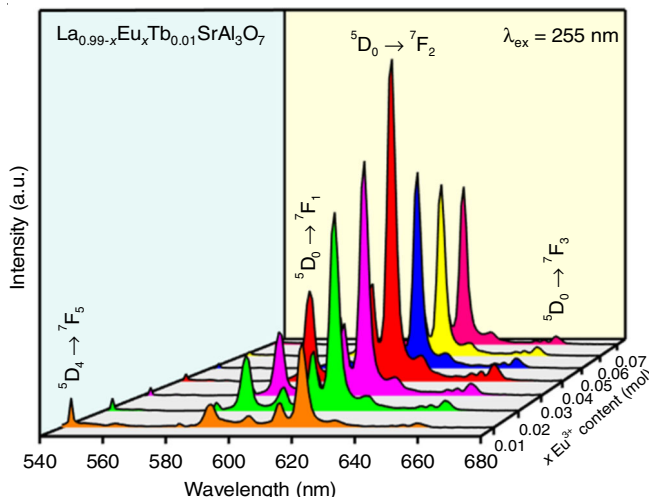


Fig. 12. Combined emission spectra of La_{0.99-x}Eu_xTb_{0.01}SrAl₃O₇ ($x = 0.01-0.07$ mol) co-doped nanocrystalline phosphors at $\lambda_{ex} = 255$ nm

excitation bands, presumably because the intensity associated with the Tb³⁺ ions transitions was significantly lower than that of the Eu³⁺ ions transitions [12,78,79].

Also, emission peak corresponding to Eu³⁺ ions along with relatively low intensity Tb³⁺ ions emission peak (at 544 nm) were clearly visible in the combined PL spectra (Fig. 12) of La_{0.99-x}Eu_xTb_{0.01}SrAl₃O₇ ($x = 0.01-0.07$ mol) nanosamples [80]. It seems vital to investigate how concentration of Eu³⁺ ions influences the co-doped phosphors emission intensity in order to ascertain the optimum Eu³⁺ ion concentration as well as the energy transfer mechanism [81,82]. As the concentration of Eu³⁺ ions (x) raised, lumen intensity of Tb³⁺ ions peak (⁵D₄ → ⁷F₅, 544 nm) gradually diminished while lumen intensity of Eu³⁺ (⁵D₀ → ⁷F₂, 617 nm) ions peak in co-doped La_{0.99-x}Eu_xTb_{0.01}SrAl₃O₇ ($x = 0.01-0.07$ mol) nanophosphor enhanced upto $x = 0.04$ mol (Eu³⁺) then decreased with very minimal surplus beyond the critical concentration as a result of concentration quenching as displayed in Fig. 13. With elevated Eu³⁺ ion concentration, the distance between doped ions diminishes leads to the enhancement of non-radiative energy exchanges between dopant ions which are responsible for this apparent concentration quenching process [83,84]. It also may be feasible to interpret the observed reduction in Tb³⁺ ion emission intensity patterns in co-doped samples as evidence of prospective energy transfer from ⁵D₄ (Tb³⁺) → ⁵D₀ (Eu³⁺) energy levels in LaSrAl₃O₇ host matrix. Fig. 14 illustrated the possible energy transfer between dopant ions (Eu³⁺ and Tb³⁺) and energy level outline to describe emission route in Eu³⁺/Tb³⁺ co-doped LaSrAl₃O₇ luminescent material [17,75,85].

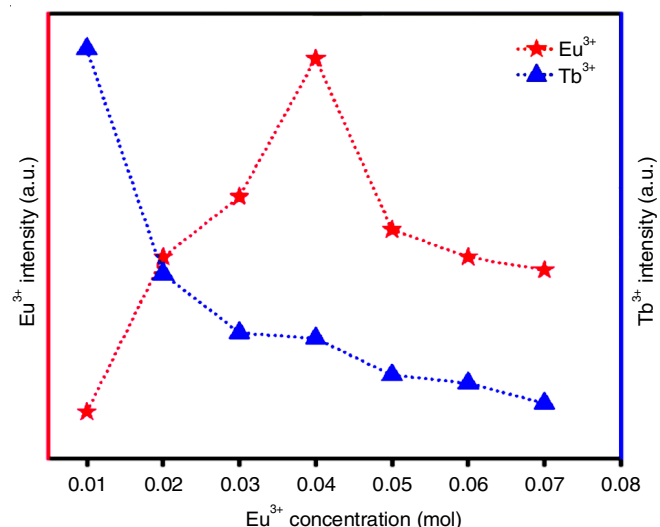


Fig. 13. Deviations in emission intensities of Eu³⁺ (⁵D₀ → ⁷F₂) and Tb³⁺ (⁵D₄ → ⁷F₅) ions with change in Eu³⁺ concentration

Generally, the non-radiative energy transfer mechanism genre possibly will be composed of the multipolar interactions or exchange interactions. If the exchange interaction seems prevailing, the critical distance (R_c) value should be less than 5 Å, otherwise, the multipolar interactions were significant [15]. For the study of the non-radiative energy transfer mechanism i.e. concentration quenching, the critical distance (R_c) can be calculated using eqn. 9 as follows [86-88]:

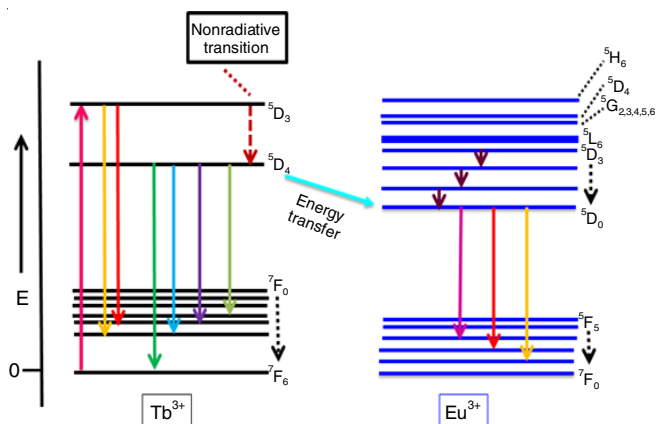


Fig. 14. Illustration depicting possible energy transfer process from $\text{Tb}^{3+} \rightarrow \text{Eu}^{3+}$ ions in $\text{LaSrAl}_3\text{O}_7$ host

$$R_c = 2 \left(\frac{3V}{4\pi x_c N} \right)^{1/3} \quad (9)$$

where V = unit cell volume (325.48 \AA^3); x_c = critical concentration of dopant Tb^{3+} and Eu^{3+} ions (0.05 mol); N = available locations for dopants in unit cell $N = 2$.

The energy transfer between the dopant ions should be regulated by the electric multipolar interaction in synthesized co-doped nanocrystalline phosphor as R_c was calculated to be 5.576 \AA [15,89]. The Dexter energy transfer equation of multipolar interaction (eqn. 10) was applied to grasp the possible mechanism for multipolar interactions between dopant ions in selected $\text{LaSrAl}_3\text{O}_7$ matrix.

$$\frac{\eta_0}{\eta} = C^n \quad (10)$$

where η_0 = sensitizer (Tb^{3+}) quantum efficiency in absence of activator; η = sensitizer (Tb^{3+}) quantum efficiency in presence of activator (Eu^{3+}); C = content quantity of sensitizer (Tb^{3+}) and activator (Eu^{3+}); $n = 6, 8$ and 10 , which are correlate to the dipole-dipole (d-d), dipole-quadrupole (d-q) and quadrupole-quadrupole (q-q) interactions, respectively.

The ratio of photoluminescence intensity (I_0/I) can be utilized to approximate the value of η_0/η ratio adopting Reisfeld's approximation. Here, I and I_0 signify luminescence intensities of sensitizer (Tb^{3+}) with and devoid of activator (Eu^{3+}), respectively. The correlated graphical representation (Fig. 15) of I_0/I versus $C^{n/3}$ demonstrated an optimal linear tandem at $n = 8$,

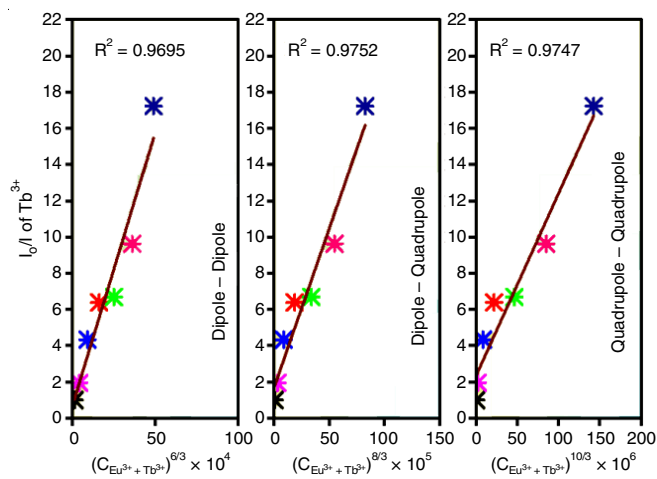


Fig. 15. Dependence of I_0/I of Tb^{3+} on $(C_{\text{Eu}^{3+}} + C_{\text{Tb}^{3+}})^{n/3}$ for $\text{Eu}^{3+}/\text{Tb}^{3+}$ co-doped $\text{LaSrAl}_3\text{O}_7$ phosphors

corresponding to dipole-quadrupole (d-q) interactions between Tb^{3+} and Eu^{3+} in $\text{LaSrAl}_3\text{O}_7$ lattice [70,75,90,91].

Colorimetric probe: The channeling of energy from a sensitizer to an activator ($\text{Tb}^{3+} \rightarrow \text{Eu}^{3+}$) opens up an avenue for achieving color-tunable emissions [15]. The CIE chromaticity coordinates using MATLAB software, color-purity (CP) and color correlated temperature (CCT) for $\text{La}_{0.99}\text{Tb}_{0.01}\text{SrAl}_3\text{O}_7$ and $\text{La}_{0.99-x}\text{Eu}_x\text{Tb}_{0.01}\text{SrAl}_3\text{O}_7$ ($x = 0.01-0.07$ mol) co-doped nanoluminescent samples were assessed on the basis of their associated spectra and summarized in Table-3. The CIE color coordinates of $\text{La}_{0.99}\text{Tb}_{0.01}\text{SrAl}_3\text{O}_7$ and $\text{La}_{0.92}\text{Eu}_{0.07}\text{Tb}_{0.01}\text{SrAl}_3\text{O}_7$ phosphors were calculated to be (0.353, 0.554) and (0.643, 0.357) which were lying in greenish and deep red zone, respectively. It is also significant that color-tunable phosphor essences ranging from greenish to orange-red to a deep red could be achieved by merging Tb^{3+} and Eu^{3+} ions in $\text{LaSrAl}_3\text{O}_7$ substrate lattice as shown in Fig. 16. Consequently, it appears evident that pig-ment emission can be tailored to a desired color range merely only altering the concentration of co-dopants (Tb^{3+} and Eu^{3+}). Further, the color purity (CP) of the produced nano-samples was ascertained using eqn. 11 by utilizing their CIE color coordinates to gauge their luminous attributes [12,92,93].

$$\text{Color purity (\%)} = \frac{\sqrt{(x-x_i)^2 + (y-y_i)^2}}{\sqrt{(x_d-x_i)^2 + (y_d-y_i)^2}} \times 100 \quad (11)$$

The resulting co-doped luminous materials revealed high color purity (80-90% assortment), signifying potential utili-

TABLE-3
DIVERSE CHROMATICITY CONSTRAINTS OF $\text{La}_{0.99}\text{Tb}_{0.01}\text{SrAl}_3\text{O}_7$ AND
 $\text{La}_{0.99-x}\text{Eu}_x\text{Tb}_{0.01}\text{SrAl}_3\text{O}_7$ ($x = 0.01-0.07$ mol) NANOCRYSTALLINE SAMPLES

Samples	CIE (x, y)	CP (%)	(u', v')	CCT (K)
$\text{La}_{0.99}\text{Tb}_{0.01}\text{SrAl}_3\text{O}_7$	0.353, 0.554	57.82	0.158, 0.558	–
$\text{La}_{0.98}\text{Eu}_{0.01}\text{Tb}_{0.01}\text{SrAl}_3\text{O}_7$	0.600, 0.399	79.99	0.364, 0.545	1714.63
$\text{La}_{0.97}\text{Eu}_{0.02}\text{Tb}_{0.01}\text{SrAl}_3\text{O}_7$	0.644, 0.356	89.22	0.431, 0.535	2356.75
$\text{La}_{0.96}\text{Eu}_{0.03}\text{Tb}_{0.01}\text{SrAl}_3\text{O}_7$	0.648, 0.350	90.13	0.438, 0.532	2500.96
$\text{La}_{0.95}\text{Eu}_{0.04}\text{Tb}_{0.01}\text{SrAl}_3\text{O}_7$	0.647, 0.352	89.89	0.436, 0.534	2471.04
$\text{La}_{0.94}\text{Eu}_{0.05}\text{Tb}_{0.01}\text{SrAl}_3\text{O}_7$	0.649, 0.351	90.39	0.439, 0.533	2531.99
$\text{La}_{0.93}\text{Eu}_{0.06}\text{Tb}_{0.01}\text{SrAl}_3\text{O}_7$	0.646, 0.354	89.68	0.434, 0.535	2410.40
$\text{La}_{0.92}\text{Eu}_{0.07}\text{Tb}_{0.01}\text{SrAl}_3\text{O}_7$	0.643, 0.357	88.99	0.428, 0.536	2312.3

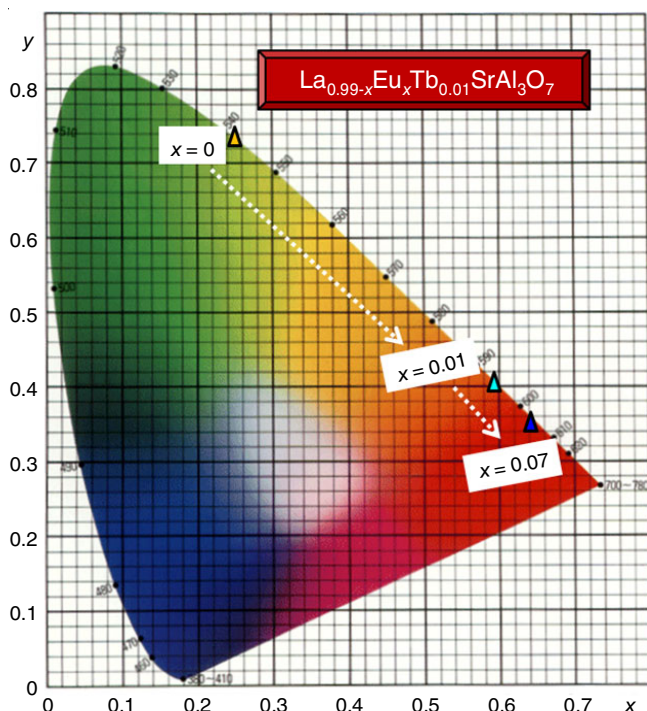


Fig. 16. CIE color coordinates of Tb³⁺ single and Eu³⁺/Tb³⁺ co-doped LaSrAl₃O₇ nanophosphors

zation of these materials in solid state lighting technologies. Also, the CCT is a key criterion for figuring out the chromatic aspects of the produced illumination in Kelvin (K). The McCamy formula (eqn. 12) was used to probe the CCT of radiance stemming by La_{0.99-x}Eu_xTb_{0.01}SrAl₃O₇ ($x = 0.01-0.07$ mol) co-doped nanocrystalline luminescent materials [94-96].

$$\text{CCT} = -437n^3 + 360n^2 - 686n + 5514.3 \quad (12)$$

where $n = (x - x_e)/(y - y_e)$ with chromaticity epicentre $x_e = 0.332$ and $y_e = 0.186$.

The following computations were engaged in the conversion of chroma (x, y to u', v') for calculating CCT values [12,97]:

$$u' = \frac{4x}{-2x + 12y + 3}; \quad v' = \frac{9y}{-2x + 12y + 3} \quad (13)$$

The insights observed for all La_{0.99-x}Eu_xTb_{0.01}SrAl₃O₇ ($x = 0.01-0.07$ mol) co-doped nanoluminescent sample pursuant to investigation validate their potential as the platform for sophisticated displays, diverse luminous sources, photonic appliances and numerous lighting devices [11,27,98,99].

Conclusion

In present work, La_{0.99-x}Eu_xTb_{0.01}SrAl₃O₇ ($x = 0.01-0.07$ mol) color tunable luminous nanocrystalline materials were synthesized using a simple, cost effective, less time consuming, self-propagating solution combustion synthesis route. The XRD pattern of synthesized La_{0.95}Eu_{0.04}Tb_{0.01}SrAl₃O₇ co-doped phosphor revealed the formation of crystalline and pure single phase at 900 °C. The synthesized co-doped phosphor sample illustrated the loosely organized bunches of spherical shaped nano-scale particles. The EDAX spectrum shows that Tb, Eu, La, Sr, Al and O elements were present in Eu³⁺/Tb³⁺ co-doped

LaSrAl₃O₇ nanophosphor. Moreover, the DR spectroscopy revealed that the band gap energy of Eu³⁺, Tb³⁺ co-doped LaSrAl₃O₇ nanophosphors lay within the range of inorganic semiconductor substances, which strengthened their potency. With altering the contrast ratio of Tb³⁺ and Eu³⁺, specific emission based on energy transfer (ET) from Tb³⁺ → Eu³⁺ was also feasible to be altered ranging from greenish to orange-red to a deep red. Under 255 nm excitation it emerged that the energy transfer was caused by a dipole-quadrupole (d-q) interaction. The observed color-tunable emission for La_{0.99-x}Eu_xTb_{0.01}SrAl₃O₇ ($x = 0.01-0.07$ mol) co-doped nanoluminescent demonstrates their future use as a foundation for sophisticated displays, diverse luminous sources, photonic appliances, pc-LEDs, full-color displays and numerous lighting devices.

ACKNOWLEDGEMENTS

The financial support from University Grants Commission, New Delhi, India in form of SRF (Award no. 271/ CSIR-UGC NET DEC. 2018) to Deepika Dhatervwal is gratefully acknowledged. The authors are thankful to Chaudhary Bansi Lal University, Bhiwani; CIL, Maharshi Dayanand University, Rohtak; CIL, Guru Jambheshwar University of Science and Technology, Hisar (India), and CIL, Chaudhary Charan Singh Haryana Agricultural University, Hisar (India), for providing the instrumentation facilities.

CONFLICT OF INTEREST

The authors declare that there is no conflict of interests regarding the publication of this article.

REFERENCES

- H. Cheng, T. Li, L. Guo, K. Zhang and C. Zhu, *J. Lumin.*, **261**, 119914 (2023); <https://doi.org/10.1016/j.jlumin.2023.119914>
- G.B. Nair, H.C. Swart and S.J. Dhole, *Prog. Mater. Sci.*, **109**, 100622 (2020); <https://doi.org/10.1016/j.pmatsci.2019.100622>
- W. Ma, J. Zhang, X. Zhang, X. Zhang, Y. Liu, S. Liao and S. Lian, *J. Alloys Compd.*, **785**, 53 (2019); <https://doi.org/10.1016/j.jallcom.2019.01.194>
- K. Rawat, A.K. Vishwakarma and K. Jha, *Opt. Laser Technol.*, **145**, 107455 (2022); <https://doi.org/10.1016/j.optlastec.2021.107455>
- X. Wu, L. Du, Q. Ren, Y. Zhao and O. Hai, *J. Solid State Chem.*, **293**, 121798 (2021); <https://doi.org/10.1016/j.jssc.2020.121798>
- G. Wu, Y. Zhang, S. Kang, Z. Yu, X. Wang, D. Jin and L. Wang, *Optik*, **229**, 166271 (2021); <https://doi.org/10.1016/j.ijleo.2021.166271>
- I.Ç. Keskin, S. Gülltekin, M.I. Kati, M. Türemis, K. Ay, Y. Arslanlar, A. Çetin and R. Kibar, *J. Alloys Compd.*, **789**, 932 (2019); <https://doi.org/10.1016/j.jallcom.2019.03.153>
- L. Fu, Y. Wu and T. Fu, *J. Lumin.*, **245**, 118758 (2022); <https://doi.org/10.1016/j.jlumin.2022.118758>
- R. Priya, O.P. Pandey and S.J. Dhole, *Opt. Laser Technol.*, **135**, 106663 (2021); <https://doi.org/10.1016/j.optlastec.2020.106663>
- M. Saif, *J. Lumin.*, **135**, 187 (2013); <https://doi.org/10.1016/j.jlumin.2012.10.022>
- D. Dhatervwal and S. Singh, *Materialia*, **20**, 101249 (2021); <https://doi.org/10.1016/j.mtla.2021.101249>

12. D. Dhatervwal, M. Matoria, A. Dalal, S. Kumar and S. Singh, *J. Struct. Chem.*, **65**, 130877 (2024); https://doi.org/10.26902/JSC_id130877
13. Q. Wu, M. Fu, C. Gu, Y. Wang, L. Yao and C. Wang, *J. Alloys Compd.*, **968**, 171909 (2023); <https://doi.org/10.1016/j.jallcom.2023.171909>
14. H.X. Chen, Y.C. Ren, Z.J. Li and Y.G. Yang, *Chem. Phys. Lett.*, **780**, 138911 (2021); <https://doi.org/10.1016/j.cplett.2021.138911>
15. R. Yang, C. Yin, Y. Gao, X. Zhou, P. Jiang, R. Cong and T. Yang, *J. Lumin.*, **231**, 117821 (2021); <https://doi.org/10.1016/j.jlumin.2020.117821>
16. M. Qu, X. Zhang, X. Mi, H. Sun, Q. Liu and Z. Bai, *J. Alloys Compd.*, **872**, 159506 (2021); <https://doi.org/10.1016/j.jallcom.2021.159506>
17. D. Xu, W. Zhou, Z. Zhang, X. Ma and Z. Xia, *Mater. Res. Bull.*, **108**, 101 (2018); <https://doi.org/10.1016/j.materresbull.2018.08.040>
18. J. He, C. Yan, M. Huang, R. Shi, Y. Chen, C.D. Ling and Z. Liu, *Chemistry*, **26**, 5619 (2020); <https://doi.org/10.1002/chem.201905607>
19. Q. Bai, Z. Wang, P. Li, S. Xu, T. Li, J. Cheng and Z. Yang, *Mater. Des.*, **108**, 597 (2016); <https://doi.org/10.1016/j.matdes.2016.07.041>
20. W. Yang, Z. Zhang, J. Niu, W. Zhou and S. Li, *Appl. Phys. A Mater. Sci. Process.*, **125**, 837 (2019); <https://doi.org/10.1007/s00339-019-3131-6>
21. E. Rai, A. Roy, A. Rai, V.J. Fulari and S.B. Rai, *J. Alloys Compd.*, **937**, 168395 (2023); <https://doi.org/10.1016/j.jallcom.2022.168395>
22. Sheetal, V.B. Taxak, Mandeep and S.P. Khatkar, *J. Alloys Compd.*, **549**, 135 (2013); <https://doi.org/10.1016/j.jallcom.2012.09.033>
23. A. Bao, C. Tao and H. Yang, *J. Mater. Sci. Mater. Electron.*, **19**, 476 (2008); <https://doi.org/10.1007/s10854-007-9366-6>
24. M.S. Mendhe, P.P. Bhure, P.C. Dhabale, S.G. Revankar and S.P. Puppallwar, *Mater. Today Proc.*, **15**, 633 (2019); <https://doi.org/10.1016/j.matpr.2019.04.131>
25. B. Wang, H. Wang, J. Huang, J. Zhou and P. Liu, *J. Am. Ceram. Soc.*, **103**, 315 (2020); <https://doi.org/10.1111/jace.16736>
26. V. Singh, S. Watanabe, T.K.G. Rao and H.Y. Kwak, *J. Fluoresc.*, **21**, 313 (2011); <https://doi.org/10.1007/s10895-010-0718-x>
27. D. Dhatervwal, M. Matoria and S. Singh, *Next Nanotechnol.*, **5**, 100033 (2024); <https://doi.org/10.1016/j.nxnano.2023.100033>
28. S. Singh, A. Dalal, M. Kumar and D. Dhatervwal, *Asian J. Chem.*, **35**, 1019 (2023); <https://doi.org/10.14233/ajchem.2023.27019>
29. A. Bao, H. Yang and C. Tao, *Curr. Appl. Phys.*, **9**, 1252 (2009); <https://doi.org/10.1016/j.cap.2009.02.008>
30. H. Dahiya, M. Dalal, J. Dalal, V.B. Taxak, S.P. Khatkar and D. Kumar, *Mater. Res. Bull.*, **99**, 86 (2018); <https://doi.org/10.1016/j.materresbull.2017.11.005>
31. Y. Li and Y. Wang, *J. Inf. Disp.*, **12**, 93 (2011); <https://doi.org/10.1080/15980316.2011.567822>
32. V. Singh, P. Halappa, N. Singh, M.S. Pathak, C. Shivakumara and V. Natarajan, *J. Electron. Mater.*, **48**, 3415 (2019); <https://doi.org/10.1007/s11664-019-07122-9>
33. X. Jin, L. Zhang, H. Luo, X. Fan, L. Jin, B. Liu, D. Li, Z. Qiu and Y. Gan, *Integr. Ferroelectr.*, **188**, 1 (2018); <https://doi.org/10.1080/10584587.2018.1454750>
34. L. Du, X. Wu, Q. Ren and O. Hai, *Polyhedron*, **200**, 115143 (2021); <https://doi.org/10.1016/j.poly.2021.115143>
35. P. Sehrawat, R.K. Malik, P. Boora, M. Punia, M. Sheoran, P. Chhillar, S.P. Khatkar and V.B. Taxak, *Chem. Phys. Lett.*, **763**, 138243 (2021); <https://doi.org/10.1016/j.cplett.2020.138243>
36. Yashaswini, S. Pratibha, N. Dhananjaya, C. Pandurangappa and R. Lokesh, *Inorg. Chem. Commun.*, **123**, 108342 (2021); <https://doi.org/10.1016/j.inoche.2020.108342>
37. D. Nath, F. Singh and R. Das, *Mater. Chem. Phys.*, **239**, 122021 (2020); <https://doi.org/10.1016/j.matchemphys.2019.122021>
38. S. Devi, A. Khatkar, V.B. Taxak, A. Hooda and S.P. Khatkar, *J. Electron. Mater.*, **51**, 3637 (2022); <https://doi.org/10.1007/s11664-022-09608-5>
39. P.P. Pal and J. Manam, *Appl. Phys. A Mater. Sci. Process.*, **116**, 213 (2014); <https://doi.org/10.1007/s00339-013-8095-3>
40. P. Kumar, S. Singh, I. Gupta, V. Kumar and D. Singh, *Optik*, **267**, 169709 (2022); <https://doi.org/10.1016/j.ijleo.2022.169709>
41. G.P. Darshan, H.B. Premkumar, H. Nagabhushana, S.C. Sharma, S.C. Prashantha, H.P. Nagaswarup and B.D. Prasad, *Dyes Pigments*, **131**, 268 (2016); <https://doi.org/10.1016/j.dyepig.2016.02.015>
42. A.K. Bedyal, D.D. Ramteke, V. Kumar and H.C. Swart, *J. Mater. Sci. Mater. Electron.*, **30**, 11714 (2019); <https://doi.org/10.1007/s10854-019-01533-4>
43. C. Kaliyaperumal, A. Sankarakumar and T. Paramasivam, *J. Alloys Compd.*, **831**, 154782 (2020); <https://doi.org/10.1016/j.jallcom.2020.154782>
44. M. Song, W. Zhao, W. Ran, J. Xue, Y. Liu and J.H. Jeong, *J. Alloys Compd.*, **803**, 1063 (2019); <https://doi.org/10.1016/j.jallcom.2019.06.379>
45. N. Verma, B. Marí, K.C. Singh, J. Jindal, S. Yadav and A. Mittal, *J. Aust. Ceram. Soc.*, **55**, 179 (2019); <https://doi.org/10.1007/s41779-018-0223-2>
46. S. Chahar, M. Dalal, S. Singh, R. Devi, V.B. Taxak and S.P. Khatkar, *J. Mater. Sci. Mater. Electron.*, **29**, 2175 (2018); <https://doi.org/10.1007/s10854-017-8130-9>
47. S. Singh, S.P. Khatkar, P. Boora and V.B. Taxak, *J. Mater. Sci.*, **49**, 4773 (2014); <https://doi.org/10.1007/s10853-014-8176-5>
48. K. Thomas, D. Alexander, S. Sisira, P.R. Biju, N.V. Unnikrishnan and C. Joseph, *Opt. Mater.*, **80**, 37 (2018); <https://doi.org/10.1016/j.optmat.2018.04.010>
49. G.D. Gesesse, A. Gomis-Berenguer, M.F. Barthe and C.O. Ania, *J. Photochem. Photobiol. Chem.*, **398**, 112622 (2020); <https://doi.org/10.1016/j.jphotochem.2020.112622>
50. L. Zhang, S. Yi, X. Hu, B. Liang, W. Zhao and Y. Wang, *Mod. Phys. Lett. B*, **31**, 1750051 (2017); <https://doi.org/10.1142/S0217984917500518>
51. P. Kubelka, *J. Opt. Soc. Am.*, **44**, 330 (1954); <https://doi.org/10.1364/JOSA.44.000330>
52. S.V. Motloug, K.G. Tshabalala, R.E. Kroon, T.T. Hlatshwayo, M. Mlambo and S. Mpelane, *J. Mol. Struct.*, **1175**, 241 (2019); <https://doi.org/10.1016/j.molstruc.2018.08.002>
53. W. Zhao, H. Wen, B. Fan and H. Li, *J. Solid State Chem.*, **288**, 121403 (2020); <https://doi.org/10.1016/j.jssc.2020.121403>
54. N. Jain, B.P. Singh, R.K. Singh, J. Singh and R.A. Singh, *J. Lumin.*, **188**, 504 (2017); <https://doi.org/10.1016/j.jlumin.2017.05.007>
55. P.K. Jisha, K.S. Sumitha, S.C. Prashantha, G. Sashikumar, S. Sabreesh, S.N. Tatvik Mahesha and C. Ravikumar, *Mater. Today Proc.*, **62**, 5700 (2022); <https://doi.org/10.1016/j.matpr.2022.05.202>
56. M. Prasad and V.K. Rai, *J. Alloys Compd.*, **911**, 164968 (2022); <https://doi.org/10.1016/j.jallcom.2022.164968>
57. A. Kumar and J. Manam, *J. Alloys Compd.*, **829**, 154610 (2020); <https://doi.org/10.1016/j.jallcom.2020.154610>
58. R. Mahajan and R. Prakash, *Mater. Chem. Phys.*, **246**, 122826 (2020); <https://doi.org/10.1016/j.matchemphys.2020.122826>
59. A.S. Ahmed, M. Shafeeq M, M.L. Singla, S. Tabassum, A.H. Naqvi and A. Azam, *J. Lumin.*, **131**, 1 (2011); <https://doi.org/10.1016/j.jlumin.2010.07.017>
60. T. Krishnapriya, A. Jose, T. Anna Jose, C. Joseph, N.V. Unnikrishnan and P.R. Biju, *Adv. Powder Technol.*, **32**, 1023 (2021); <https://doi.org/10.1016/j.apt.2021.02.003>
61. M. Venugopal, H.P. Kumar and R. Jayakrishnan, *J. Electroceram.*, **44**, 163 (2020); <https://doi.org/10.1007/s10832-020-00207-6>

62. G. Wu, H.M. Deng, N.F. Ding, H.R. Yan, P.X. Yang and J.H. Chu, *Mater. Sci. Forum*, **745-746**, 136 (2013); <https://doi.org/10.4028/www.scientific.net/MSF.745-746.136>
63. M.K. Halimah, M.F. Faznny, M.N. Azlan and H.A.A. Sidek, *Results Phys.*, **7**, 581 (2017); <https://doi.org/10.1016/j.rinp.2017.01.014>
64. P. Kumar, D. Singh, I. Gupta, S. Singh, S. Nehra and R. Kumar, *Mater. Chem. Phys.*, **301**, 127610 (2023); <https://doi.org/10.1016/j.matchemphys.2023.127610>
65. G.V.L. Reddy, L.R. Moorthy, T. Chengaiah and B.C. Jamalaiah, *Ceram. Int.*, **40**, 3399 (2014); <https://doi.org/10.1016/j.ceramint.2013.09.092>
66. X. Liu, Y. Lü, C. Chen, S. Luo, Y. Zeng, X. Zhang, M. Shang, C. Li and J. Lin, *J. Phys. Chem. C*, **118**, 27516 (2014); <https://doi.org/10.1021/jp508773t>
67. E.B. Shaik, B.V.N. Kumar, S.K. Chirauri and K.R. Rao, *J. Mater. Sci. Mater. Electron.*, **33**, 105 (2022); <https://doi.org/10.1007/s10854-021-07257-8>
68. X. Wu, J. Zheng, Q. Ren, J. Zhu, Y. Ren and O. Hai, *J. Alloys Compd.*, **805**, 12 (2019); <https://doi.org/10.1016/j.jallcom.2019.07.061>
69. B. Li, Y. Liu, Y. Lu, X. Zhang, F. Song and F. Yang, *J. Mater. Sci. Mater. Electron.*, **26**, 5618 (2015); <https://doi.org/10.1007/s10854-015-3111-3>
70. W. Xie, J. Feng, X. Liu, L. Yan, H. Guo, Y. Dai, Y. Xie, H.S. Jang and J. Lin, *J. Alloys Compd.*, **753**, 781 (2018); <https://doi.org/10.1016/j.jallcom.2018.04.260>
71. K. Park, H. Kim and D.A. Hakeem, *Ceram. Int.*, **42**, 10526 (2016); <https://doi.org/10.1016/j.ceramint.2016.03.150>
72. J. Wang, X. Peng, D. Cheng, Z. Zheng and H. Guo, *J. Rare Earths*, **39**, 284 (2021); <https://doi.org/10.1016/j.jre.2020.06.010>
73. L. Han, C. Guo, Y. Ning, L. Zhao and Z. Ci, *J. Lumin.*, **237**, 118184 (2021); <https://doi.org/10.1016/j.jlumin.2021.118184>
74. J. Li, Z. Zhang, X. Li, Y. Xu, Y. Ai, J. Yan, J. Shi and M. Wu, *J. Mater. Chem. C Mater. Opt. Electron. Devices*, **5**, 6294 (2017); <https://doi.org/10.1039/C7TC01285C>
75. S.K. Jaganathan, J.P. Anthuvan and I.B.S. Banu, *J. Mater. Sci. Mater. Electron.*, **29**, 2363 (2018); <https://doi.org/10.1007/s10854-017-8155-0>
76. W. Sun, H. Li, B. Li, J. Du, J. Hao, C. Hu, Y. Wang, X. Yi, R. Pang and C. Li, *J. Mater. Sci. Mater. Electron.*, **30**, 9421 (2019); <https://doi.org/10.1007/s10854-019-01272-6>
77. M.J. Xu, J.Y. Si, G.H. Li, Y.J. Liu, G.M. Cai and J. Zhang, *J. Lumin.*, **221**, 117115 (2020); <https://doi.org/10.1016/j.jlumin.2020.117115>
78. G. Li, Y. Wang, Y. Wei and X. Wang, *J. Mater. Sci. Mater. Electron.*, **31**, 3835 (2020); <https://doi.org/10.1007/s10854-020-02918-6>
79. D. Yang, L. Liao, Q. Guo, L. Mei, H. Liu, T. Zhou and H. Ye, *RSC Adv.*, **9**, 4295 (2019); <https://doi.org/10.1039/C8RA10059D>
80. S. Nan, F. Hong, H. Xu, J. Dou, G. Liu, X. Dong, J. Wang and W. Yu, *J. Mater. Sci. Mater. Electron.*, **31**, 13688 (2020); <https://doi.org/10.1007/s10854-020-03926-2>
81. B. Yu, B. Zheng, H. Xia, J. Wang, H. Song and B. Chen, *Ceram. Int.*, **47**, 9668 (2021); <https://doi.org/10.1016/j.ceramint.2020.12.106>
82. T. Wang, Q. Shi, K.V. Ivanovskikh, L. Wang, H. Guo, P. Huang and C. Cui, *J. Lumin.*, **236**, 118138 (2021); <https://doi.org/10.1016/j.jlumin.2021.118138>
83. G.B. Nair and S.J. Dhoble, *RSC Adv.*, **5**, 49235 (2015); <https://doi.org/10.1039/C5RA07306E>
84. B. Li, X. Huang, H. Guo and Y. Zeng, *Dyes Pigments*, **150**, 67 (2018); <https://doi.org/10.1016/j.dyepig.2017.11.003>
85. Z. Fan, Y. Qie, D. Guo, Y. Liu, F. Kong, Z. Shi and H. Yang, *J. Mater. Sci. Mater. Electron.*, **32**, 210 (2021); <https://doi.org/10.1007/s10854-020-04756-y>
86. G. Blasse, *Phys. Lett. A*, **28**, 444 (1968); [https://doi.org/10.1016/0375-9601\(68\)90486-6](https://doi.org/10.1016/0375-9601(68)90486-6)
87. G. Blasse, *J. Solid State Chem.*, **62**, 207 (1986); [https://doi.org/10.1016/0022-4596\(86\)90233-1](https://doi.org/10.1016/0022-4596(86)90233-1)
88. B. Shen, F. Wu, Y. Zhang, H. Xia, B. Chen and J. Hu, *J. Alloys Compd.*, **809**, 151836 (2019); <https://doi.org/10.1016/j.jallcom.2019.151836>
89. M. Dalal, V.B. Taxak, S. Chahar, J. Dalal, A. Khatkar and S.P. Khatkar, *J. Alloys Compd.*, **686**, 366 (2016); <https://doi.org/10.1016/j.jallcom.2016.06.040>
90. L. Li, X. Tang, Z. Wu, Y. Zheng, S. Jiang, X. Tang, G. Xiang and X. Zhou, *J. Alloys Compd.*, **780**, 266 (2019); <https://doi.org/10.1016/j.jallcom.2018.11.378>
91. J. Niu, N. Sos, Z. Zhang and W. Zhou, *Opt. Mater.*, **97**, 109397 (2019); <https://doi.org/10.1016/j.optmat.2019.109397>
92. K.N. Kumar, L. Vijayalakshmi, J. Choi and J.S. Kim, *J. Alloys Compd.*, **787**, 711 (2019); <https://doi.org/10.1016/j.jallcom.2019.02.105>
93. H. Duan, R. Cui, X. Qi and C. Deng, *J. Mol. Struct.*, **1205**, 127551 (2020); <https://doi.org/10.1016/j.molstruc.2019.127551>
94. S. Devi, V.B. Taxak, D. Sangwan, A. Hooda and S.P. Khatkar, *J. Mater. Sci. Mater. Electron.*, **33**, 5983 (2022); <https://doi.org/10.1007/s10854-022-07778-w>
95. P.K. Jisha, R. Naik, S.C. Prashantha, H. Nagabhushana, S.C. Sharma, H.P. Nagaswarupa, K.S. Anantharaju, B.D. Prasad and H.B. Premkumar, *J. Lumin.*, **163**, 47 (2015); <https://doi.org/10.1016/j.jlumin.2015.03.006>
96. K.N. Kumar, L. Vijayalakshmi and J.S. Kim, *Mater. Res. Bull.*, **103**, 234 (2018); <https://doi.org/10.1016/j.materresbull.2018.03.045>
97. I. Gupta, D. Singh, S. Singh, P. Kumar, S. Bhagwan and V. Kumar, *Chem. Phys. Lett.*, **814**, 140350 (2023); <https://doi.org/10.1016/j.cplett.2023.140350>
98. R.K. Sajwan, S. Tiwari, T. Harshit and A.K. Singh, *Opt. Quantum Electron.*, **49**, 344 (2017); <https://doi.org/10.1007/s11082-017-1158-5>
99. X. Huang, B. Li, P. Du, H. Guo, R. Cao, J.S. Yu, K. Wang and X.W. Sun, *Dyes Pigments*, **151**, 202 (2018); <https://doi.org/10.1016/j.dyepig.2017.12.067>